

# Synthesis of highly ordered mesoporous silica thin films for nano-fabrication of platinum nanodot arrays

Yoko Kumai · Noriaki Sugimoto · Hiroshi Tsukada · Shinji Inagaki

Published online: 6 August 2009  
© Springer Science+Business Media, LLC 2009

**Abstract** Mesoporous silica thin films with highly ordered cubic  $Pm\text{-}3n$  and three dimensional hexagonal  $P6_3/mmc$  symmetries were synthesized by evaporation induced self assembly (EISA) method controlling the ratio of HCl and tetramethoxysilane in the initial sol solution and the humidity in the dip-coating chamber. Using these optimized mesoporous silica thin films, highly ordered Pt nanodot arrays with cubic and three dimensional hexagonal symmetries were synthesized by simple immersion in a Pt precursor solution and photoreduction. These periodic nanodot arrays in the silica thin film have a potential to be applied to single-electron devices mediated by coupling interactions with neighboring nanodots.

**Keywords** Nanostructures · Mesopore · Thin film · Nanodots

## 1 Introduction

Ordered mesoporous silicas [1–3] have attracted significant attention for their useful applications, to catalysis and absorption but also as templates for fabrication of nano-devices, due to their tunable pore size and pore-arrangement

structure. To date, a variety of nanoparticles and nanowires of Pt [4–10], Ag [11–14], Pd [8, 15] and Au [7, 8] as well as  $\text{Fe}_2\text{O}_3$  [14] and  $\text{In}_2\text{O}_3$  [16] metal oxides, have been synthesized using mesoporous powders or thin films. In most cases, the pores were partially filled with materials, and nanoparticles and wires were randomly distributed in the mesoporous silica matrices. Recently, the syntheses of ordered nanoparticle arrays of CdS [17], Au [18], and Pt [18] in mesoporous silica films have been reported. Fan et al. reported the synthesis of gold nanocrystal/silica mesostructured thin films with cubic symmetry ( $Fm\bar{3}m$ ) via self-assembly of water-soluble nanocrystal micelles with soluble silica [19]. These periodic nanodot arrays in silica thin films could be applied to single-electron devices mediated by coupling interactions with neighboring nanodots. An ordered lattice and perfect packing of dots are very important for three dimensional (3D) arrays of multi-tunnel junctions, and it should be possible to control the properties of single-electron devices by changing the pore size and arrangement in the mesoporous silica thin films. Very recently, we reported the synthesis of a highly ordered Pt nanodot array with cubic symmetry, simply by immersing a mesoporous silica thin film into a Pt-precursor solution followed by photoreduction [20]. The cages of mesoporous thin films were filled with Pt nanoparticles of approximately 4 nm diameter, and ordered cubic-lattice arrays of nanodots were obtained. In conventional mesoporous films (fabricated without optimized synthesis conditions), the order of the pore arrangement is insufficient, and structural defects have been observed in some cases.

Here, we report the optimization of the synthesis conditions of mesoporous silica thin films with highly ordered cubic  $Pm\text{-}3n$  and 3D-hexagonal  $P6_3/mmc$  symmetries, and the formation of highly ordered Pt nanodot arrays by using the optimized films. The structural ordering

Y. Kumai (✉) · N. Sugimoto · H. Tsukada · S. Inagaki  
Toyota Central R&D Labs., Inc., 41-1 Yokomichi Nagakute,  
Aichi 480-1192, Japan  
e-mail: kumai@mosk.tylabs.co.jp

N. Sugimoto  
e-mail: e0961@mosk.tylabs.co.jp

H. Tsukada  
e-mail: e1066@mosk.tylabs.co.jp

S. Inagaki  
e-mail: inagaki@mosk.tylabs.co.jp

of the mesostructured films strongly depended on the HCl/Si ratio in the initial sol solution and on the humidity level in the dip-coating chamber. Grosso et al. have reported extensive studies on the synthesis conditions of mesoporous silica thin films including HCl content in the initial sol-solution [21] and humidity in the dip-coating chamber [22, 23]. However, there are no reports on detailed studies on the relationship between structural ordering and these conditions.

## 2 Experimental

### 2.1 Preparation of mesoporous silica thin films

Mesoporous silica thin films were prepared by sol-gel synthesis under acidic conditions. Tetramethoxysilane (TMOS), purchased from Tri Chemical Labs., Inc., was employed as the silicon source. Octadecyltrimethylammonium chloride (ODTMA), purchased from Tokyo Chemical Industry Co., Ltd., was used as a surfactant template. For the syntheses of cubic (*Pm-3n*) mesoporous silica, 2N HCl (100–1250 µL) and H<sub>2</sub>O (50 mL) were added to the TMOS (15.22 g), and the mixtures were stirred for 1 h at room temperature to yield the first solution. ODTMA (5.80 g) was dissolved in a mixture of EtOH (20 mL), H<sub>2</sub>O (30 mL) and 12N HCl (100 µL). The mixtures were added to the TMOS solutions and stirred for a further 40 min to yield silica/surfactant sol-solutions. The final molar ratios of the mixtures for cubic films were TMOS:ODTMA:HCl:H<sub>2</sub>O:EtOH = 1:0.17:0.0022–0.0041:19:3.4. For the synthesis of hexagonal (*P6<sub>3</sub>/mmc*) mesoporous silica, 2N HCl (50–500 µL) and H<sub>2</sub>O (30 mL) were added to the TMOS (15.22 g), and the mixtures were stirred for 1 h at room temperature to yield the first solution. ODTMA (3.41 g) was dissolved in a mixture of EtOH (20 mL), H<sub>2</sub>O (10 mL) and 2N HCl (100 µL). The mixtures were added to the first solutions and stirred for a further 40 min to yield silica/surfactant sol-solutions. The molar ratios of the mixtures for hexagonal films were TMOS:ODTMA:HCl:H<sub>2</sub>O:EtOH = 1:0.10:0.0021–0.0034:7.7:3.4. The sol-solutions were dip-coated onto a silicon wafer with a constant withdrawal speed of 20 mm/min. The humidity in the dip-coating chamber was kept at 5%, 35% (40% for cubic) or 70% (75% for cubic) relative humidity. For the pretreatment to clean the surface, the silicon wafers were immersed in a HF solution (HF:H<sub>2</sub>O = 1:50 volume ratio) for 1 min at 298 K and rinsed with ion-exchanged water and distilled water, and then dried. The silica/surfactant thin film on the Si substrates were dried at room temperature for 24 h and then at 373 K for 1 h. Finally, the films were calcined in air at 673 K for 4 h to remove the surfactant and accelerate the condensation of the silica framework.

### 2.2 Preparation of Pt nanoparticles in the mesoporous silica thin films

H<sub>2</sub>PtCl<sub>6</sub> aqueous solution (15 wt%) was purchased from Tanaka Kikinzoku Kogyo. The mesoporous silica on Si substrates were dried under vacuum for 24 h and immersed into a platinum precursor solution of 15% H<sub>2</sub>PtCl<sub>6</sub>:EtOH:H<sub>2</sub>O = 1:2:2 by volume. Ultrasonic irradiation was used for an initial 10 min, and then the film was kept in the solution for 24 h. The H<sub>2</sub>PtCl<sub>6</sub>/mesoporous film composites were placed in a vacuum-cell equipped with a quartz glass window and dried under vacuum for 24 h. After evacuation, methanol vapor (10 Torr) and H<sub>2</sub>O vapor (10 Torr) were introduced in the vacuum-cell. The H<sub>2</sub>PtCl<sub>6</sub>/mesoporous film in the vacuum-cell was irradiated with UV light (300–600 nm) for 72 h to reduce H<sub>2</sub>PtCl<sub>6</sub> to platinum metal. The Pt particles were deposited not only in the cages in the film, but also on the surface of the film. The Pt particles deposited on the film were removed by wiping with soft tissue paper before HRTEM and XRD measurements.

### 2.3 Measurements

X-ray diffraction (XRD) patterns of the films were obtained using a Rigaku Rint-2200 diffractometer using Cu K $\alpha$  radiation. Transmission electron microscopy (TEM) images were obtained with a JEOL JEM2000EX instrument. Film thickness was measured using the ULVAC Dektak 3ST instrument. The samples for TEM were scratched off and microtome-cut mesoporous thin film on the substrate.

## 3 Results and discussion

### 3.1 Optimization of synthesis conditions

Cubic and hexagonal mesophases were prepared at typical conditions of ODTMA/TMOS of 0.17 and 0.10, respectively [24]. We found that the HCl/TMOS ratio in the initial mixture and the humidity in the dip-coating chamber were crucial factors to improve structural ordering of the mesoporous silica thin films. Figure 1 shows XRD patterns of surfactant-free mesoporous silica thin films prepared at different HCl/TMOS ratios. The figure shows diffraction patterns in a low angle, assigned to cubic symmetry with a lattice constant of  $a = 76.3 \text{ \AA}$  (Fig. 1a) and hexagonal symmetry with lattice constants of  $a = 44.9 \text{ \AA}$ ,  $c = 20.2 \text{ \AA}$  (Fig. 1b), respectively. The HCl/TMOS ratio affected the peak intensities sensitively for both mesophases. Figure 2 plots the peak intensities of 210 for the cubic phase and 100 for the hexagonal phase as a function of the HCl/TMOS ratio. Maximum peak intensities at

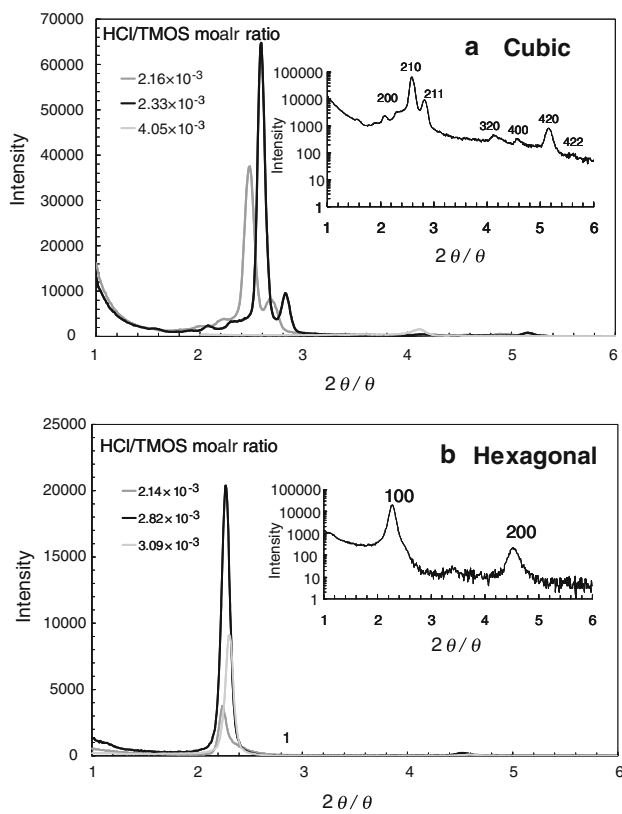


**Fig. 1** XRD patterns of typical calcined mesoporous thin films with **a** cubic ( $\text{HCl}/\text{TMOS}$  molar ratio =  $2.16 \times 10^{-3}$ ,  $2.33 \times 10^{-3}$ ,  $4.05 \times 10^{-3}$ ) and **b** hexagonal ( $\text{HCl}/\text{TMOS}$  molar ratio =  $2.14 \times 10^{-3}$ ,  $2.82 \times 10^{-3}$ ,  $3.09 \times 10^{-3}$ ) symmetries

$\text{HCl}/\text{TMOS}$  ratios of 0.0023 and 0.0028 for the cubic and hexagonal mesophases, respectively, were obtained. As the film thicknesses are almost constant (cubic: 380–420 nm, hexagonal: 480–530 nm), the highest intensity indicates the highest structural ordering of the mesoporous thin film. An increase in the  $\text{HCl}/\text{TMOS}$  ratio accelerates the hydrolysis and condensation rates of the TMOS precursor [21]. A high degree of hydrolysis of the TMOS precursor is appropriate to form ordered mesostructures due to the effective interaction between hydrolyzed TMOS species and surfactant ions. However, too much condensation of precursor is not appropriate because highly polymerized silicate species is difficult to organize into the ordered mesostructure.

Next, we studied the effects of humidity in the dip-coating chamber. Figure 3 shows the XRD patterns of mesoporous silica thin films with cubic and hexagonal mesophases prepared under humidities of 5, 35, 70% and 5, 42, 74% respectively at the optimized  $\text{HCl}/\text{TMOS}$  ratios. Figure 4 plots the peak intensities of 210 and 100 diffractions as a function of humidity in the dip-coating chamber. The peak intensities increased at high humidity conditions. The film thicknesses were almost constant

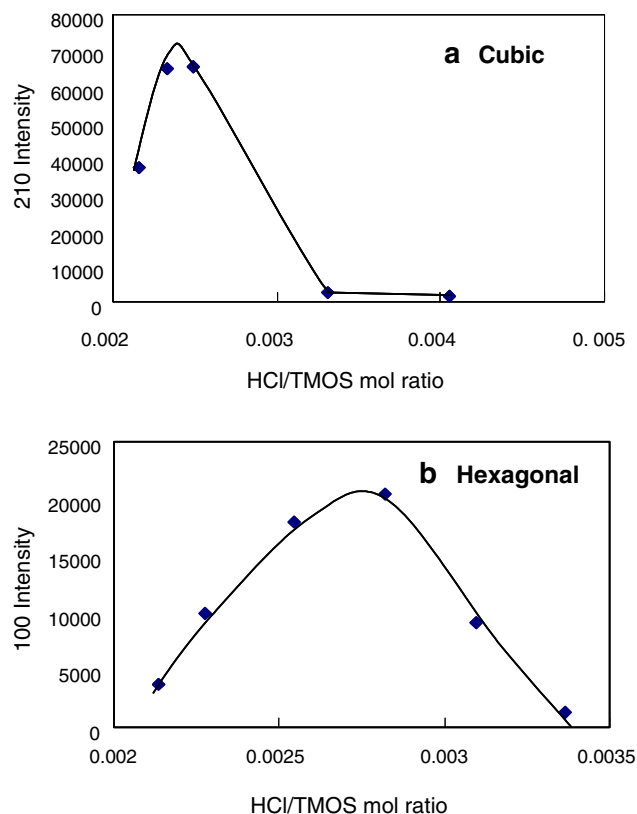


**Fig. 2** Relationship between XRD peak intensity and  $\text{HCl}/\text{TMOS}$  ratio for **a** cubic (210 peak) and **b** hexagonal (100 peak) films

between 400 and 560 nm for the cubic mesophase and between 480 and 750 nm for the hexagonal mesophase. The solvent-evaporation from the substrate after dip-coating was slow at high humidity conditions [23]. The slow evaporation would be appropriate to form a highly ordered mesostructure because it would easily reach the equilibrium state of the ordered micelle structure in the film during the solvent evaporation.

### 3.2 TEM observations

TEM of the mesoporous silica thin films prepared at the optimized condition showed clear images of highly ordered mesostructures of cubic ( $Pm-3n$ ) and hexagonal ( $P6_3/mmc$ ) symmetries, as shown in Figs. 5 and 6, respectively. The samples which were scratched off the cubic mesoporous thin film on the substrate show lattice images along [100] (Fig. 5a), [210] (Fig. 5b) and a mixture of [100] and [210] (Fig. 5c). Mesoporous materials with cubic  $Pm-3n$  symmetry consist of two types of cages, A- and B-cages, wherein the A-cage is larger than the B-cage. The TEM images clearly show ordered arrangements of the A- and B-cages. The single domain size was estimated to be 200–600 nm from the TEM image (Fig. 5c, d). The domains

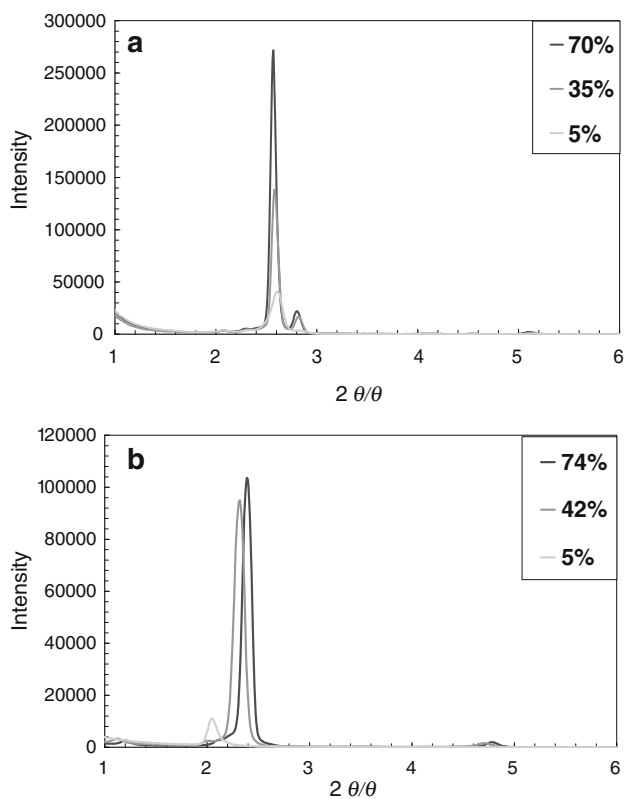


**Fig. 3** XRD patterns of calcined mesoporous films with cubic (**a**) and hexagonal (**b**) symmetry prepared under various relative humidity conditions in the dip-coating chamber

were closely packed and there is almost no gap among the domains. A cross-section of the cubic film on the substrate, prepared by microtome-cutting, shows a single crystal-like uniform lattice image from the bottom to the top of the film, as shown in Fig. 5d.

The hexagonal thin films also show a highly ordered pore-arrangement structure. The samples which were

**Fig. 5** TEM images of cubic ( $Pm-3n$ ) mesoporous silica thin films. Plan-view of [100] (**a**), [210] (**b**), [100] + [210] (**c**), and cross-sectional image (**d**)

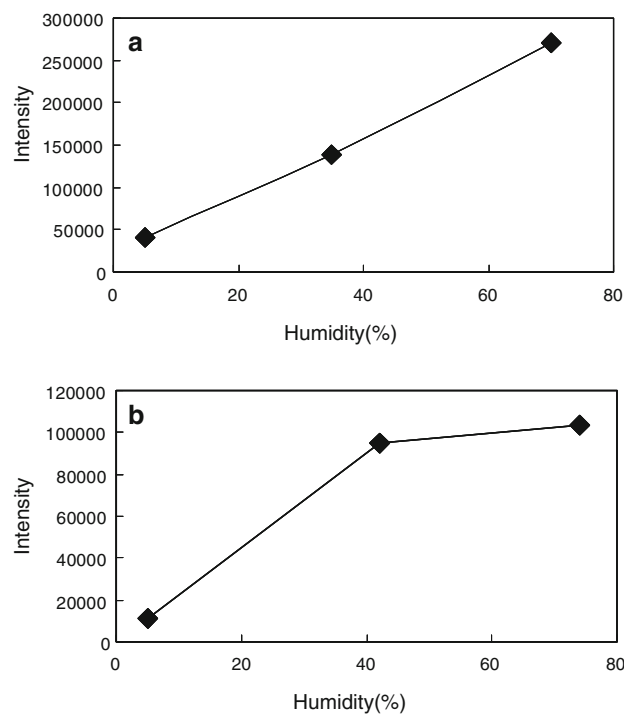
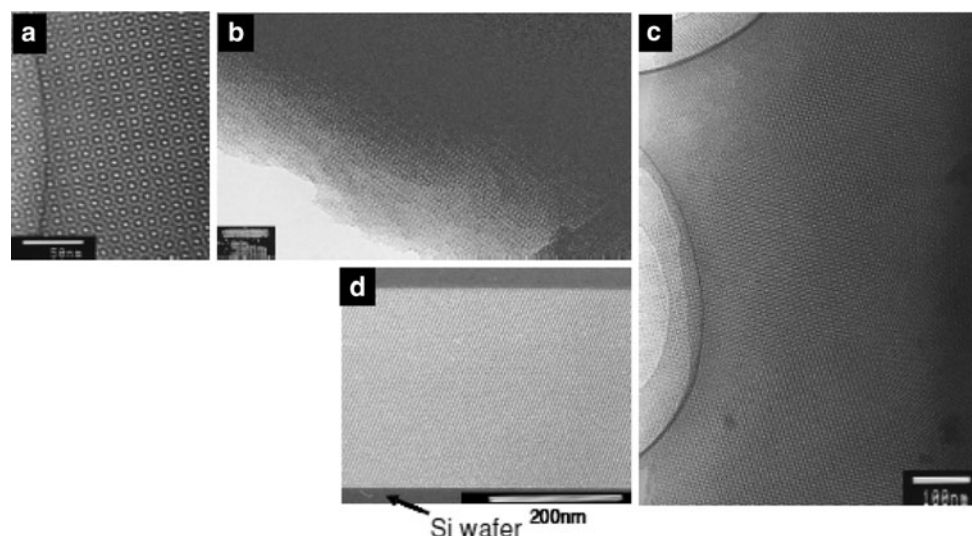


**Fig. 4** Relationship between the XRD peak intensity and the relative humidity in the dip-coating chamber for **a** cubic (210 peak) and **b** hexagonal (100 peak) films

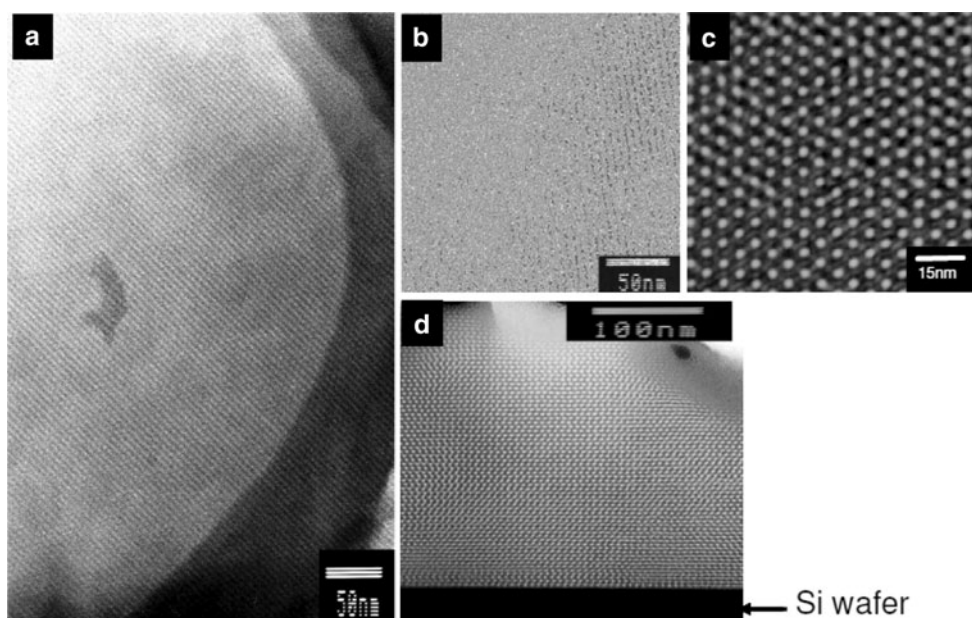
scratched off the hexagonal mesoporous thin film on the substrate show lattice images along [110] (Fig. 6a, b) and [100] (Fig. 6c). The single domain size was estimated to be 300–500 nm at least from the TEM images (Fig. 6a, d). There is almost no gap among the domains.

### 3.3 Pt nanoparticles in mesoporous silica thin films

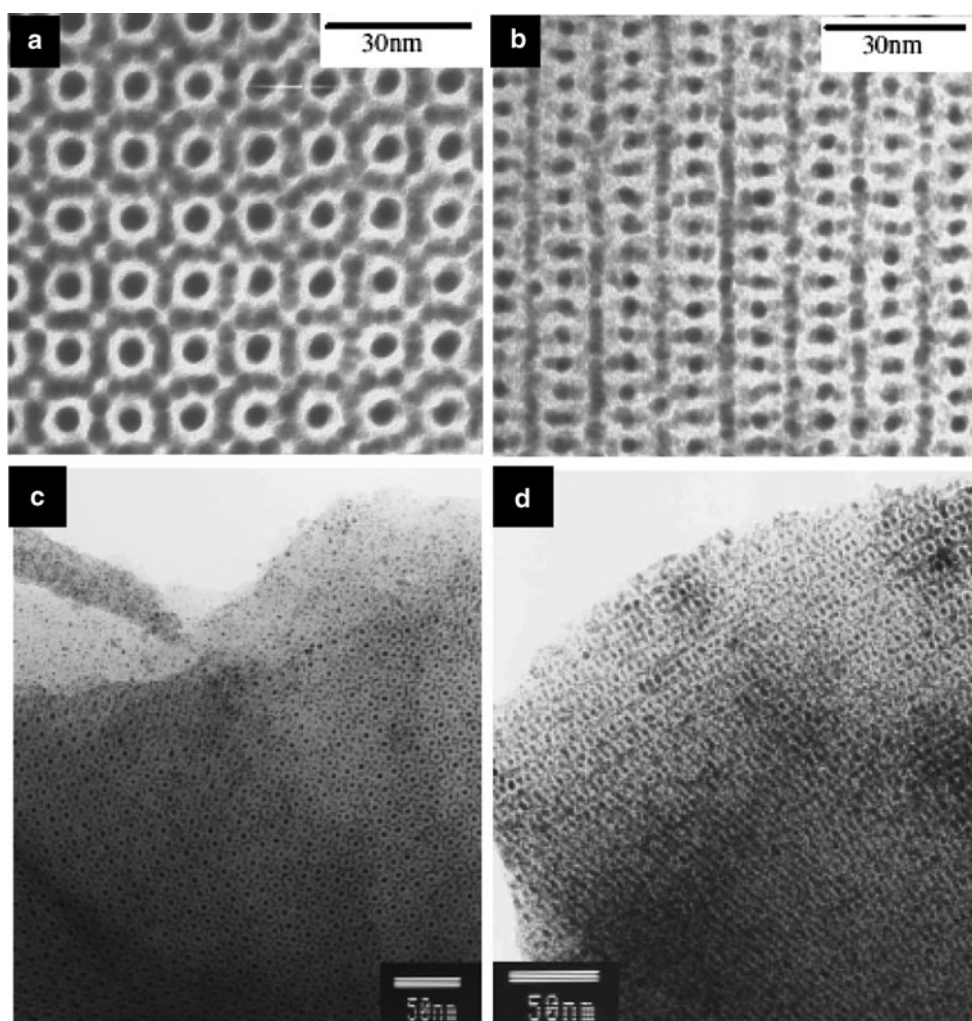
Figure 7 shows TEM images of Pt-filled mesoporous silica thin films with cubic mesophase. Figure 7a, c show lattice



**Fig. 6** TEM images of 3D-hexagonal ( $P6_3/mmc$ ) mesoporous silica thin films. Plan-view of [110] (a, b), [100] (c), and cross-sectional image (d)



**Fig. 7** HRTEM images of Pt/mesoporous silica thin films [100] (a, c) and [210] (b, d) of cubic ( $Pm-3n$ )



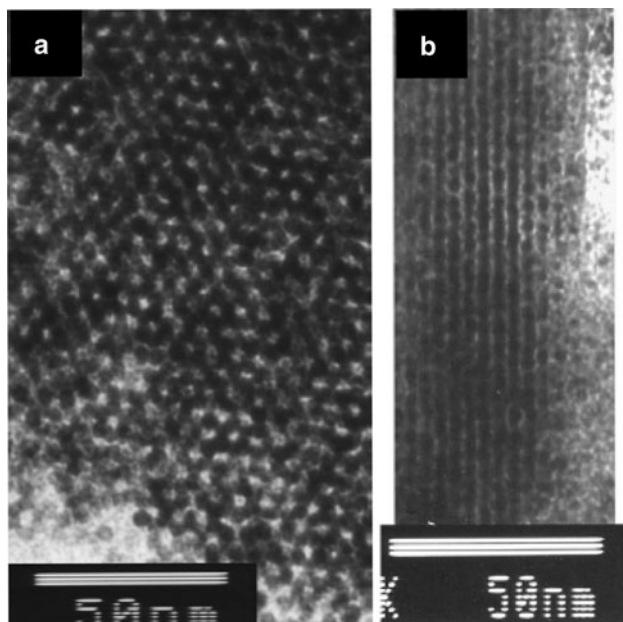


**Fig. 8** HRTEM images of Pt/mesoporous silica thin films of [100] (**a**) and [110] (**b**) of 3D-hexagonal ( $P6_3/mmc$ )

images along [100] and Fig. 7b, d show [210] of cubic ( $Pm-3n$ ). The cages of the highly ordered mesoporous thin films are filled with Pt over a large area of the thin films. As we reported the detail in last article [20], both the A- and B-cages of the cubic mesoporous thin film were filled with the Pt nanoparticles, and an ordered cubic-lattice array of nanodots was obtained. The particle size of the Pt was determined to be approximately 4 nm in diameter, which is in good agreement with the pore sizes in the mesoporous silica thin films. Also, the particle size of Pt was estimated to be 2.7 nm from the XRD pattern using the Scherrer equation.

Figure 8 shows TEM images of Pt-filled mesoporous silica thin films with hexagonal mesophase. They show not so clear images of ordered arrangements of Pt nanoparticles compared to the films with cubic mesophases. It would be attributable to decrease in the structural order of the mesoporous film during the formation of Pt nanoparticles.

#### 4 Conclusions

We optimized the synthesis conditions of highly ordered mesoporous silica thin films with cubic and 3D-hexagonal symmetries. The HCl/TMOS ratio of the initial sol solution and the humidity in the dip-coating chamber are crucial factors to improve the structural ordering of the cubic and 3D-hexagonal films. Using these optimized mesoporous

thin films, ordered Pt nanodot arrays with cubic and 3D-hexagonal symmetries were synthesized. These periodic nanodot arrays in the silica thin films have a potential to be applied to single-electron devices mediated by coupling interactions with neighboring nanodots.

#### References

1. C.T. Kresge, M.E. Leonowicz, W.J. Roth, J.C. Vartuli, J.C. Beck, *Nature* **359**, 710 (1992)
2. T. Yanagisawa, T. Shimizu, K. Kuroda, C. Kato, *Bull. Chem. Soc. Jpn.* **63**, 988 (1990)
3. S. Inagaki, Y. Fukushima, K. Kuroda, *J. Chem. Soc., Chem. Commun.* 680 (1993)
4. C.H. Ko, R. Ryoo, *Chem. Commun.* 2467 (1996)
5. M. Sasaki, M. Osada, N. Sugimoto, S. Inagaki, Y. Fukushima, A. Fukuoka, M. Ichikawa, *Microporous Mesoporous Mater.* **21**, 597 (1998)
6. Z. Liu, Y. Sakamoto, T. Ohsuna, T. Hiraga, O. Terasaki, C.H. Ko, H.J. Shin, R. Ryoo, *Angew. Chem. Int. Ed.* **39**, 3107 (2000)
7. H.J. Shin, R. Ryoo, Z. Liu, O. Terasaki, *J. Am. Chem. Soc.* **123**, 1246 (2001)
8. Y. Han, J.M. Kim, G.D. Stucky, *Chem. Mater.* **12**, 2068 (2000)
9. A. Fukuoka, H. Araki, J. Kimura, Y. Sakamoto, T. Higuchi, N. Sugimoto, S. Inagaki, M. Ichikawa, *J. Mater. Chem.* **14**, 752 (2004)
10. A. Fukuoka, Y. Sakamoto, S. Guan, S. Inagaki, N. Sugimoto, Y. Fukushima, K. Hirahara, S. Iijima, M. Ichikawa, *J. Am. Chem. Soc.* **123**, 3373 (2001)
11. M.H. Huang, A. Choudrey, P. Yang, *Chem. Commun.* 1063 (2000)
12. J. Plyuto, J. Berquier, C. Jacquiod, *Chem. Commun.* 1653 (1999)
13. S. Besson, T. Gacoin, C. Ricolleau, J.P. Boilot, *Chem. Commun.* 360 (2003)
14. M. Fröba, R. Kohn, G. Bouffaud, O. Richard, G. Tendeloo, *Chem. Mater.* **11**, 2858 (1999)
15. H. Kang, Y.W. Jun, J.I. Park, K.B. Lee, J. Cheon, *Chem. Mater.* **12**, 3530 (2000)
16. H. Yang, Q. Shi, B. Tian, Q. Lu, F. Gao, S. Xie, J. Fan, C. Yu, B. Tu, D. Zhao, *J. Am. Chem. Soc.* **125**, 4724 (2003)
17. S. Besson, T. Bacoin, C. Ricolleau, C. Jacquiod, J.P. Boilot, *Nano Lett.* **2**, 409 (2002)
18. A. Fukuoka, H. Araki, Y. Sakamoto, N. Sugimoto, H. Tsukada, Y. Kumai, Y. Akimoto, M. Ichikawa, *Nano Lett.* **2**, 793 (2002)
19. H. Fan, K. Yang, D.M. Boye, T. Sigmon, K.J. Malloy, H. Xu, G.P. Lopez, C.J. Brinker, *Science* **304**, 567 (2004)
20. Y. Kumai, H. Tsukada, Y. Akimoto, N. Sugimoto, Y. Seno, A. Fukuoka, M. Ichikawa, S. Inagaki, *Adv. Mater.* **18**, 760 (2006)
21. D. Grossso, F. Cangol, G.J.A.A. Soler-Illia, E.L. Crepaldi, H. Amenitsch, A. Brunet-Brunneau, A. Bourgeois, C. Sanchez, *Adv. Funct. Mater.* **14**, 309 (2004)
22. F. Cangol, D. Grossso, G.J.A.A. Soler-Illia, E.L. Crepaldi, F. Babonneau, H. Amenitsch, C.J. Sanchez, *J. Mater. Chem.* **13**, 61 (2003)
23. A. Gibaud, D. Grossso, B. Smarsly, A. Baptiste, J.F. Bardeau, F. Babonneau, D.A. Doshi, Z. Chen, C.J. Brinker, C. Sanchez, *J. Phys. Chem. B* **107**, 6114 (2003)
24. D. Grossso, A.R. Balkende, P.A. Albouy, M. Lavergne, L. Mazerolle, F. Babonneau, *J. Mater. Chem.* **10**, 2085 (2000)